



Review

Recent Advances of Upconversion Nanomaterials in the Biological Field

Cunjin Gao¹, Pengrui Zheng¹, Quanyao Liu¹, Shuang Han¹, Dongli Li¹, Shiyong Luo¹, Hunter Temple², Christina Xing², Jigang Wang^{1,*}, Yanling Wei^{3,*}, Tao Jiang^{4,*} and Wei Chen^{2,5,*}

- ¹ Beijing Key Laboratory of Printing and Packaging Materials and Technology, Beijing Institute of Graphic Communication, Beijing 102600, China; gcj2019015220@163.com (C.G.); zhengpengrui9999@126.com (P.Z.); drllqx@163.com (Q.L.); 13552797385@163.com (S.H.); lidongli@bigc.edu.cn (D.L.); luoshiyong@bigc.edu.cn (S.L.)
- ² Department of Physics, The University of Texas at Arlington, Arlington, TX 76019-0059, USA; hunter.temple@uta.edu (H.T.); Christina.Xing@uta.edu (C.X.)
- ³ Faculty of Applied Sciences, Jilin Engineering Normal University, Changchun 130052, China
- ⁴ CAS Center for Excellence in Nanoscience, Beijing Key Laboratory of Micro-Nano Energy and Sensor, Beijing Institute of Nanoenergy and Nanosystems, Chinese Academy of Sciences, Beijing 101400, China
- ⁵ Medical Technology Research Centre, Chelmsford Campus, Anglia Ruskin University, Chelmsford CM1 1SQ, UK
- * Correspondence: jigangwang@bigc.edu.cn (J.W.); weiyanning@jleu.edu.cn (Y.W.); jiangtao@binn.cas.cn (T.J.); weichen@uta.edu (W.C.)

Abstract: Rare Earth Upconversion nanoparticles (UCNPs) are a type of material that emits high-energy photons by absorbing two or more low-energy photons caused by the anti-stokes process. It can emit ultraviolet (UV) visible light or near-infrared (NIR) luminescence upon NIR light excitation. Due to its excellent physical and chemical properties, including exceptional optical stability, narrow emission band, enormous Anti-Stokes spectral shift, high light penetration in biological tissues, long luminescent lifetime, and a high signal-to-noise ratio, it shows a prodigious application potential for bio-imaging and photodynamic therapy. This paper will briefly introduce the physical mechanism of upconversion luminescence (UCL) and focus on their research progress and achievements in bio-imaging, bio-detection, and photodynamic therapy.

Keywords: UCNPs; UCL; RE-doped; bio-imaging; PDT; bio-detection



Citation: Gao, C.; Zheng, P.; Liu, Q.; Han, S.; Li, D.; Luo, S.; Temple, H.; Xing, C.; Wang, J.; Wei, Y.; et al. Recent Advances of Upconversion Nanomaterials in the Biological Field. *Nanomaterials* **2021**, *11*, 2474. <https://doi.org/10.3390/nano11102474>

Academic Editor: Julia Pérez-Prieto

Received: 4 September 2021

Accepted: 15 September 2021

Published: 22 September 2021

Publisher's Note: MDPI stays neutral with regard to jurisdictional claims in published maps and institutional affiliations.



Copyright: © 2021 by the authors. Licensee MDPI, Basel, Switzerland. This article is an open access article distributed under the terms and conditions of the Creative Commons Attribution (CC BY) license (<https://creativecommons.org/licenses/by/4.0/>).

1. Introduction

Luminescent materials are functional materials that absorb incident energy and subsequently emit incident energy in photons. Most luminescent materials, including organic dyes and quantum dots (QDs) [1], follow Stokes Law. They absorb high-energy photons and emit low-energy photons (energy reduction), known as downconversion materials [2–7]. On the contrary, UCNPs relate to the conversion of long-wavelength NIR light with lower energy into ultraviolet or visible light with higher energy. This process is also known as the anti-stokes process, which is so-called the UCL phenomenon.

When almost all the trivalent rare earth ions (RE³⁺) are excited externally, the rare earth elements of 15 lanthanides, yttrium, and scandium can move between different energy levels, because they have a unique 4f electron configuration energy level, such as shown in Figure 1. In addition, due to the shielding of the secondary 5s²5p⁶ shell, the external environment has little effect on rare earth ions [8–11]. Under near infrared (NIR) laser irradiation, typical lanthanide-doped upconversion nanoparticles exhibit anti-Stokes shifted visible light and ultraviolet light emission, while the autofluorescence background is minimal, and the light scattering of biological tissues is greatly reduced. The reduction in light scattering caused by this near-infrared excitation will make the penetration depth of biological tissues far greater than the penetration depth under ultraviolet or visible

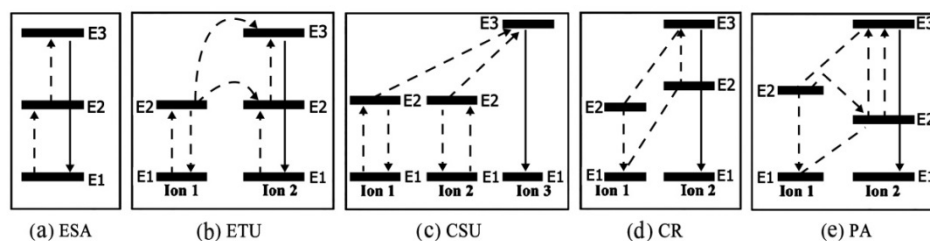


Figure 2. Upconversion mechanisms of RE-doped UCNPs: (a) ESA, (b) ETU, (c) CSU, (d) CR and (e) PA.

2.2. Energy Transfer Upconversion (ETU)

Unlike ESA, Energy transfer upconversion (ETU) involves two identical or different ions. In this photophysical process, ion 1 transitions from the ground state to E2 by absorbing excitation light; then the absorbed photon energy is transferred to the ground state E1 and excited state E2 of ion 2, so that they are excited again, while ion 1 relaxes back to ground state E1. In this process, the quantum yield of upconversion largely depends on the average distance between ion 1 and ion 2, and is mainly determined by the concentration of doped rare earth ions. The ETU process is the most important photophysical process in upconversion luminescence, because so far, the use of upconversion nanoparticles for therapeutic diagnostics and other applications is through the sensitizer Yb^{3+} , which has a strong absorption of the excitation light at 975 nm, thus making activators (Er^{3+} , etc.) produce more efficient fluorescence emission [40–45].

Moreover, the scattering and absorption of biological tissues at 975 nm are relatively small, and no optical interference occurs. Here, Yb^{3+} has a very good effect as a sensitizer because it has a sufficiently large absorption cross-section in the near-infrared region of about 975 nm. In addition, since Yb^{3+} has only two energy levels, its optimal concentration can be maintained at a high level (20–100% for fluorinated nanoparticles) without causing harmful cross-relaxation. To date, most research has focused on the development of Yb^{3+} sensitized upconversion nanoparticles pumped at about 975 nm. Using lanthanide ions themselves as sensitizers, high-efficiency ETU can also be observed in single lanthanide doping systems, for example, long-wavelength 1490 nm excitation of Er^{3+} -doped LiYF_4 [46]; or doping under 1200 nm excitation NaGdF_4 nanoparticles doped with Ho^{3+} [47]. The use of other sensitizers can be used to quench and enhance the luminous intensity of certain emission bands. For example, Nd^{3+} , Ce^{3+} , and Ho^{3+} are used as sensitizers to enhance the blue emission band of Tm^{3+} , the red emission band of Ho^{3+} , and the near-infrared emission band of Tm^{3+} , respectively [48–51].

2.3. Cooperative Sensitization Upconversion (CSU)

Cooperative sensitization upconversion (CSU) in Figure 2c is a photophysical process of the interaction of three rare earth ions (two types). Ion 1 and ion 3 usually belong to the same sensitizer, such as Yb^{3+} . After being excited by light, ion 1 and ion 3 transition to an excited state. However, ion 1 or ion 3 alone cannot excite ion 2, because their excited state energy levels are quite different, so ion 1 and ion 3 need to be co-excited to produce a virtual excited state energy level that can be compared with the excited state energy level of ion 2. The ion 2 absorbs the energy of cooperative sensitization and emits a higher energy photon. The photophysical process of CSU is often uncommon, because the energy transfer efficiency is low, and the para-virtual pair energy levels in the transfer process are involved. These energy levels must be described by quantum mechanics in higher disturbances. Nevertheless, limiting the excitation to compensate for the low efficiency provides a possibility to achieve high-resolution imaging, which is not possible with other upconversion mechanisms. At present, the CSU mechanism of $\text{Yb}^{3+}/\text{Tb}^{3+}$ [52], $\text{Yb}^{3+}/\text{Eu}^{3+}$ [53], $\text{Yb}^{3+}/\text{Pr}^{3+}$ [54] ion pairs has been reported.

2.4. Cross-Relaxation (CR)

The CR process involves two identical or different ions. In the CR process, ion 1 transfers part of the energy of the E2 energy level to ion 2, causing ion 2 to transfer to a higher excited state, while ion 1 returns to a lower energy level through a non-radiative relaxation process (Figure 2d). Although CR is related to the concentration quenching effect, it can be used to adjust the emission spectra of UCNPs. The related studies currently reported include $\text{Y}_2\text{O}_3: \text{Yb}^{3+}/\text{Er}^{3+}$ [55], $\text{GdPO}_4: \text{Sm}^{3+}$ [56], $\text{KYF}_4: \text{Tb}^{3+}, \text{Yb}^{3+}$ [57], etc.

2.5. Photon Avalanche (PA)

PA includes ESA process and CR process. Photon avalanche (PA) in Figure 2e is a process of upconversion above a certain excitation power threshold. Once excited, the upconversion fluorescence luminescence intensity will increase by orders of magnitude. In addition, the excited state energy levels of rare earth ions are also required to have a relatively high lifetime. In this process, the CR process mentioned above is also required. Ion 2 transitions from E2 back to E1 and releases energy at the same time. Ion 1 absorbs the energy and transitions from E1 to E2, and then transfers the energy to the E1 energy level of ion 2. At this time, the E1 energy level of ion 2 will absorb photons through the ESA process, which increases the population of the E1 energy level exponentially, leading to the PA process. This photophysical process is often uncommon because of the higher excitation power density required. $\text{Er}^{3+}/\text{Yb}^{3+}$ co-doped $\text{NaBi}(\text{WO}_4)_2$ phosphor produces strong green upconversion luminescence through the photon avalanche process [58]. Under excitation at 980 nm, the seven-photon PA upconversion (UC) behavior of Er^{3+} ions and four-photon NIR emission [59].

3. Synthesis Strategy and Surface Modification of UCNPs

The luminescence properties of upconversion nanomaterials are closely related to their preparation methods. Different preparation methods will affect the size, morphology, and corresponding microstructure of luminescent materials, making their application directions more diversified. Among them, thermal decomposition, hydrothermal decomposition, and co-precipitation are the three most commonly used methods, and their advantages and limitations are shown in Table 1. Other synthesis methods, including sol-gel method and combustion method, are also discussed for comparison [60–63].

Table 1. Advantages and disadvantages of upconversion nanoparticles synthesized by different methods and examples.

Method	Advantages	Disadvantages	Examples
Thermal Decomposition	Large product volume; small size distribution	The equipment is expensive; the precursor is sensitive to air; toxic by-products	ReF_3 (Re = Y,La) [64] NaLuF_4 [65] NaYbF_4 [65] MF_2 (M = Ca,Sr,Ba) [66] LiYF_4 [67] NaGdF_4 [68] BaREF_5 (RE = Y,Gd) [69] KY_3F_{10} [70] RE_2O_3 (RE = Y,La,Gd) [71] REOF (RE = Y,La,Gd) [72]
			REF_3 (RE = Y,La,Ce,Gd) [73] MF_2 (M = Ca,Sr,Ba) [74] NaYF_4 [75] NaLaF_4 [76] NaLuF_4 [77] KMnF_4 [78] BaGdF_5 [79] RE_2O_3 (RE = Y,Gd,Er) [80] LaOF [81] REPO_4 (RE = Ga,Yb,Lu) [82]
Hydrothermal Decomposition	Inexpensive precursors; no need for post-processing; precise size and shape control	Need an autoclave; the reaction process is unobservable and uncontrollable	

Table 1. Cont.

Method	Advantages	Disadvantages	Examples
Co-precipitation	Fast synthesis speed; inexpensive equipment and safe precursors	Need post-processing	NaYF ₄ [83] NaGdF ₄ [84] NaTbF ₄ [85] NaLuF ₄ [86] KGdF ₄ [87] CaF ₂ [88] LaF ₃ [89] NaScF ₄ [90]
Sol-gel Method	Inexpensive precursors; small product size	The precursor preparation process is complicated; product is easy to reunite	BaIn ₂ O ₄ :Yb ³⁺ /Tm ³⁺ /RE ³⁺ (RE = Er ³⁺ , Ho ³⁺) [91] NaPbLa (MoO ₄) ₃ : Er ³⁺ /Yb ³⁺ [92] La ₄ Ti ₃ O ₁₂ [93] Gd ₂ O ₃ : Er ³⁺ /Yb ³⁺ /Bi ³⁺ [94] CaTi ₄ O ₉ : Er ³⁺ /Yb ³⁺ [95]
Combustion Method	Fast synthesis speed; energy saving; controllable product quantity	Expensive equipment; high temperature; the particle size of the material is large and easy to agglomerate	Ba ₅ (PO ₄) ₃ OH: Er ³⁺ /Yb ³⁺ [96] Na ₃ Y(PO ₄) ₂ : Er ³⁺ /Yb ³⁺ [97] BaLaAlO ₄ :Er ³⁺ /Yb ³⁺ [98] ZrO ₂ : Ho ³⁺ /Yb ³⁺ [99] LaO ₃ : Er ³⁺ /Tm ³⁺ [100]

3.1. Thermal Decomposition Method

The thermal decomposition method is based on the high-temperature decomposition of organometallic precursors (such as metal trifluoroacetate) in high-boiling organic solvents (such as 1-octadecene). Surfactants are long-chain hydrocarbons and functional groups, such as -COOH, -NH₂ or -PO₃H (such as oleic acid, oleyl amine, trioctyl phosphine and trioctyl phosphine oxide), which are used as ligands, thus preventing the aggregation of nanoparticles. This method was originally developed by Professor Yan and others for the synthesis of LaF₃ nanoparticles [64], and later extended to the synthesis of high-quality NaYF₄ upconversion nanoparticles [65]. Capobianco et al. used trifluoroacetate precursors to synthesize Yb, Er and Yb, Tm co-doped NaYF₄ nanoparticles [101,102]. The asymmetric molecular structure of octadecene (with a high boiling point of 315 °C) is used as a solvent, and oleic acid is used as a passivation ligand. Based on the separation of nucleation and growth of nanocrystals, an improved method has been developed [100], that is, the precursor is slowly added, followed by heating, to synthesize highly monodispersed nanoparticles. Using the same strategy, Murray and colleagues prepared hexagonal NaYF₄:Yb,Er nanoparticle bodies, and precisely controlled their morphology and size [103]. Lim et al. The NaGdF₄:Er³⁺/Yb³⁺ colloidal particles with an average particle size of 32 nm were successfully synthesized by the thermal decomposition method. The prepared phosphor shows bright green upconversion luminescence under a 976 nm semiconductor laser. Phosphor particles increase the scattering of optical coherence tomography (OCT) scanning radiation, thereby observing higher image contrast [104]. So far, this method has been widely used to synthesize a series of upconversion fluoride and oxyfluoride nanoparticles (Table 1). Although this method can produce high-quality upconversion nanoparticles, it also has some disadvantages, including expensive materials, air-sensitive precursors, and the production of toxic byproducts (such as hydrogen fluoride). Recently, the Pu team reported a safe and environmentally friendly method to replace octadecene (ODE) with paraffin liquid as a high-boiling non-coordinating solvent [105]. This method is biologically cheaper and sustainable.

3.2. Hydrothermal Method

Hydrothermal synthesis is another cheap method to obtain high-quality nanocrystals. This process is usually carried out at high pressure and high temperature above the boiling point or even the critical point. A special container called autoclave is used. The main disadvantages are the opacity of the reactor and the lack of in-situ reaction process and mechanism research. On the other hand, the advantages of high crystallinity, good dispersion, and no post-treatment make it one of the most popular synthesis technologies of lanthanum-doped nanoparticles. Organic ligands/surfactants such as oleic acid [106], ethylenediamine tetraacetic acid [107,108], cetyltrimethylammonium bromide [107], and polyethyleneimine [109] are added together with precursors to achieve synchronous control of size, morphology, crystalline phase, and surface properties. For example, Zhao and colleagues reported the hydrothermal process of oleic acid mediated upconversion NaYF₄ nanocrystal synthesis, which has different shapes and morphology, including nanotubes, nanorods, and flower patterned nano disks [110]. Liu et al., used Ga³⁺ doping method to control the crystal phase [111]. They found that after on adding Ga³⁺ (accurately controlling the concentration), the required reaction temperature and time were greatly reduced, and the ultra-small NaYF₄ upconversion nanoparticles underwent a rapid cubic to hexagonal phase transition. Li et al., demonstrated a synthesis strategy of multiphase, interface controlled monodisperse nanoparticles based on Liquid-Solid-Solid transfer and separation mechanism [112]. With some improvements, this method is also used for the preparation of upconversion nanoparticles with different fluorine and oxyfluorine contents (Table 1).

3.3. Co-Precipitation Method

Among the various methods of preparing nanocrystals, the co-precipitation method is the most promising technology, providing a convenient, safe, and economical method for preparing ultra-small and monodisperse upconversion nanoparticles, without the need for expensive equipment and toxic chemicals. These nanoparticles usually need post-treatment (calcination or annealing) to improve the crystallinity of the material. This method was first used by Veggel et al. for the synthesis of lanthanide ions (Eu, Er, Nd, and Ho) doped LaF₃ downconversion nanoparticles [113]. Yi et al., subsequently demonstrated the application of this method in the preparation of upconversion nanoparticles. They used water-soluble precursors and octadecyl dithiophosphoric acid restriction ligands to prepare ultra-small (5 nm) monodisperse nanoparticles [89]. Guo et al. synthesized monodisperse NaYF₄:Yb,Er upconversion nanoparticles of different sizes (37–166 nm) by adjusting the molar ratio of ethylenediaminetetraacetic acid to total lanthanides [114]. They also found that annealing these nanoparticles at a temperature of 400–600 °C can achieve a great increase in luminous intensity (up to 40 times). Recently, Huang et al.'s team prepared Sc³⁺-doped upconversion nanoparticles by lanthanide ion precipitation in the presence of oleic acid and octadecene [90]. They found that the crystalline phase transition depends on the volume ratio of oleic acid to octadecene, through the intermediate monoclinic/hexagonal coexisting phase (oleic acid:octadecene = 3:9), from the pure monoclinic phase Na₃ScF₆ (Oleic acid: octadecene = 3:17) to pure hexagonal phase NaScF₄ (oleic acid: octadecene = 3:7). Due to the small radius of Sc³⁺, the emission of Na_xScF_{3+x}:Yb,Er is quite different from that of NaYF₄:Yb,Er, which can extend the application range of upconversion luminescent nanoparticles from optical communication to disease diagnosis.

3.4. Sol–Gel Method

The sol–gel method uses metal organics or inorganic salts as the matrix, generates gelatin through the process of hydrolysis and polycondensation, and then is dried or sintered to obtain UCNP. It has been successfully applied to the preparation of thin film coatings and glass materials for upconversion luminescent materials [115,116], but usually requires high-temperature post-processing to improve its crystallinity in order to obtain better luminescence effects. Prasad and colleagues first prepared erbium-doped ZrO₂ nanoparticles using sol-latex-gel technology [115]. However, the size of UCNP is difficult

4.1. Silica Coating

Surface silanization (or coated silica coating) is an inorganic surface treatment strategy that can make nanoparticles have water solubility and biocompatibility. It is known that silica is highly stable, biocompatible, and optically transparent. When used as a coating material, the method of surface silanization can flexibly provide abundant functional groups (such as $-\text{COOH}$, $-\text{NH}_2$, $-\text{SH}$, etc.) to meet the various needs of binding with biomolecules. Wang's group reported that the surface of UCNP is coated with polyhedral oligomeric silsesquioxane (POSS) to make the particles highly hydrophobic. They also described the preparation of liquid marbles based on optically and magnetically active dual-functional UCNPs, and their use as microreactors for the study of photodynamic therapy of cancer cells [134]. Veggel et al., reported the synthesis of SiO_2 -coated $\text{LaF}_3:\text{Yb}^{3+}/\text{Er}^{3+}$ UCNPs using the Stöber method, and the thickness of the silica shell was controlled below 15 nm [135].

4.2. Ligand Exchange

Ligand exchange is a surface modification method that replaces the original hydrophobic ligands with some hydrophilic ligands without significantly affecting the chemical and optical properties of UCNP itself. Chow's group prepared oil-soluble upconversion luminescent nanocrystals by pyrolysis, which are wrapped by oleylamine molecules. Then they exchanged ligands with dicarboxylic acid polyethylene glycol polymers and oleylamine molecules on the surface. Hydrophilic dicarboxylic acid PEG molecules can not only convert nanocrystals into water-soluble form, but also further couple the surface carboxyl groups with biomolecules [136]. Murray and colleagues reported the use of nitrosotetrafluoroborate (NOBF_4) to replace the OA and OM ligands attached to the surface of nanoparticles, so that the nanoparticles can exist stably in a variety of polar media for a long time without producing aggregation or precipitation [137].

4.3. Ligand Oxidation

Ligand oxidation is another effective method to obtain water-soluble UCNP based on the selective oxidation of surface carbon-carbon double bonds ($\text{R}-\text{CH}=\text{CH}-\text{R}'$). This method requires the presence of unsaturated bonds in the original ligand. For example, the OA ligand on the surface of UCNPs can be oxidized to azelaic acid ($\text{HOOC}(\text{CH}_2)_7\text{COOH}$), thereby making UCNP a hydrophilic material. Li's group uses *m*-chloroperoxybenzoic acid as an epoxidizing reagent to oxidize the oleic acid ligand with carbon double bonds on the surface to a ternary epoxy compound, and then interact with organic molecules containing active functional groups (such as MPEG-oh) to carry out a ring-opening reaction. Hydrophilic molecules are grafted onto oleic acid molecules to form the water-soluble conversion of luminescent nanoparticles [133]. Yan et al. used a clean and easily available strong oxidant ozone to oxidize the OA on the surface of UCNPs to azelaaldehyde or azelaic acid through ozone decomposition under certain conditions [138]. However, the ligand oxidation method has disadvantages such as long time and low efficiency, which is not conducive to actual production.

4.4. Ligand Attraction

The amphiphilic substance with both hydrophilic and hydrophobic functional groups acts on the surface of the nanoparticles. The hydrophobic functional groups in the substance are adsorbed by the oleic acid ligands on the surface of UCNPs through hydrophobic interaction, while the hydrophilic functional groups act as surface modification. Yi et al., first synthesized $\text{NaYF}_4:\text{Yb}/\text{Er}@\text{NaYF}_4$ upconversion luminescent nanoparticles with surface oleylamine modified by thermal decomposition method, using polyacrylic acid embedded with octylamine and isopropylamine as modifiers, using the hydrophobicity of polymer molecules. The hydrophobic interaction between the octyl and isopropyl groups of the UCNPs and the hydrophobic hydrocarbon groups on the surface of the UCNPs makes the

polymer coat the surface of the UCNPs. The carboxyl groups in the polymer molecules make the hydrophobic UCNPs hydrophilic, realizing the resistance to UCNPs.

4.5. Layer-by-Layer Assembly

Layer-by-layer assembly involves the electrostatic adsorption of oppositely charged anions or cations on the UCNP surface. Electrostatic attraction is one of the strongest and most stable interactions known in nature. Specific layer-by-layer modification usually contributes to the specific biological applications of UCNP. The advantage of this method is that it can prepare coated colloids of different shapes and sizes, with uniform layers of different compositions and controllable thickness [139]. Most importantly, this method can control the surface potential, size, and incorporated functional group ligands of UCNP, which is very important for cell internalization and biological targeting. Polyacrylic acid (PAA) coated with Yi groups on the surface of upconversion luminescent nanocrystals by the layer assembly method. PAA contains 25% octylamino groups and 40% isopropylamine groups, which can transfer oil-soluble upconversion luminescent nanocrystals to the water phase and further couple with biomolecules [140].

In addition to the improvement of biocompatibility, surface modification can also improve the optical properties of UCNPs, laying a foundation for the further application of UCNPs in bioimaging and other fields.

5. Biological Applications of UCNPs

Compared with traditional luminescent materials (including organic dyes and quantum dots), UCNPs have the advantages of high chemical stability, good optical stability, and narrow band gap emission. In addition, under the excitation of near-infrared light, it has strong biological tissue penetration, no damage to biological tissue, high signal-to-noise ratio, and has been widely used in the biological field. This paper also focuses on the application of up conversion luminescent materials in biological imaging, biological detection, and photodynamic therapy [141,142].

For highly infiltrative cancers, including glioblastoma multiform (GBM), it cannot be resected completely. Routinely, the conventional direct introduction to UCNPs suspension into the tissue will cause a series of biocompatibility problems. Thus, implantation of optical fiber has a heavy burden on the patient's body and a high risk of infection. Daniel et al. [143] reported the fabrication of an optical-guided UCNPs implant. Comparatively, the highly biocompatible UCNPs implant is placed into the brain via craniotomy and sealed. Then, the NIR light source passes through the healed scalp and points in the implant to stimulate the UCNPs implant, which will emit visible light to target the photosensitive metabolite protoporphyrin-IX (PpIX) in brain tumors. The flexible light guide with FEP coating approved by the FDA can also maintain NIR to visible light spectrum transduction when the implant is bent to 90°, as shown in Figure 4a. The tumor size of PDT-treated mice was significantly smaller than untreated mice, as shown in Figure 4b. Implant-based UCNPs also allow them to recover from the tissue when they are no longer needed, which cannot be achieved by direct injection of UCNPs suspension into the tissue. A wide range of emission spectrum can be engineered into UCNPs so that the implant can activate multiple drugs simultaneously without cross-interference.

Wang et al. [144] reported a method that can change intracellular pH UCNP@ZIF + TPP + PA nanometer material. The intracellular pH is usually weakly alkaline, which is not conducive to the application of acid-responsive nanomaterials. The proposed new nanomaterials (UCNP@ZIF + TPP + PA) were designed with NaYF₄: Yb: Tm (UCNPs) inner core coated by the framework of porous imidazolium zeolite (ZIF-8) for co-loading of photoacid (PA) and acid-responsive porphyrin (TPP). With 980 nm laser irradiation, the emission light of UCNPs activated PA to release H⁺. In the new acidic environment, TPP was protonated to increase its water solubility and reduce its aggregation. Simultaneously, transformed UV Vis also activates protonated TPP, which produces more singlet oxygen (¹O₂) to kill cancer

cells, to enhance the therapeutic effect of photodynamic therapy (PDT); the synthesis route and therapeutic principle are shown in Figure 5.

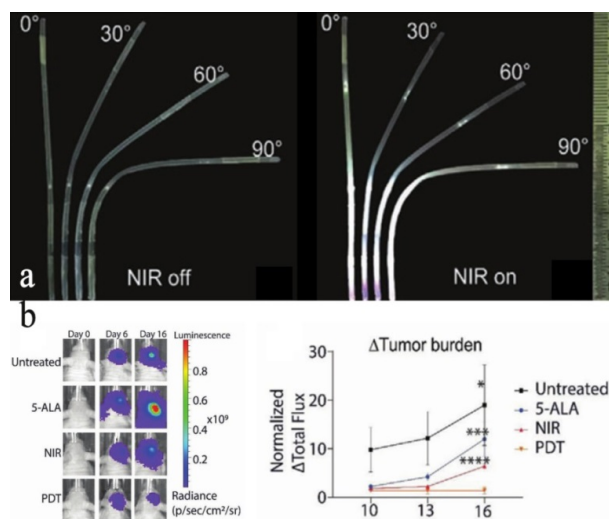


Figure 4. (a) UCNPs implant when not excited with NIR and emission intensities visualization at different angles of UCNP implant bending, excited with 1583 mW cm^{-2} of NIR. (b) IVIS imaging indicates that PDT mouse tumors were regressing, as compared to other control groups. The normalized change of tumor burden in all experiment groups over time ($n = 5$ mice/group. * $p = 0.0327$, *** $p = 0.0002$, **** $p < 0.0001$. Two-way analysis of variance (ANOVA) with Bonferroni's multiple comparison test), reprinted with permission from ref. [143]. Copyright 2020 John Wiley and Sons.

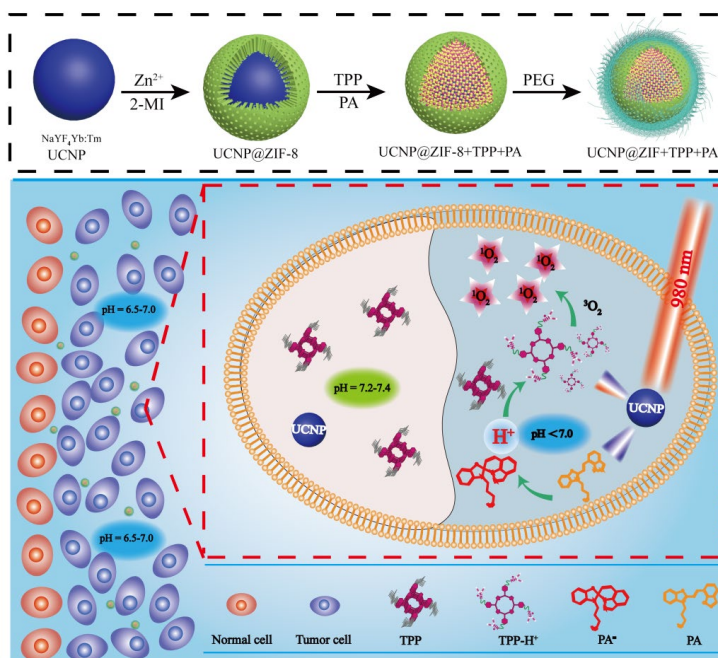


Figure 5. Synthetic route and anticancer mechanism of UCNP@ZIF + TPP + PA. Responding to weak acid tumor microenvironment, UCNP@ZIF + TPP + PA released TPP. When acid-responsive TPP entered the weak alkaline cell, it aggregated again. With 980 nm light irradiation, UCNP emitted UV-Vis light. Photoacid absorbed UV-Vis light and changed its structure to produce H⁺, which restructured the intracellular pH value. In the new weak pH, the aggregation of TPP was decreased by its protonation. Meanwhile, protonated TPP was activated by the transformed UV-Vis light and produced more ¹O₂ for enhancing PDT, reprinted with permission from ref. [144]. Copyright 2014 Royal Society of Chemistry.

One of the key challenges in the process of PDT therapy is the accurate killing of cancer cells without destroying normal cells to achieve the desired therapeutic effect. Li et al. [145] designed a type of upconversion nanoprobe (mUCNPs) for intracellular cathepsin B (CaB) reactive PDT, composed of multi-shell upconversion nanoparticles $\text{NaYF}_4: \text{Gd}@\text{NaYF}_4: \text{Er}, \text{Yb}@\text{NaYF}_4: \text{Nd}, \text{Yb}$, with the function of in situ self-tuning therapy effect prediction, as shown in Figure 6.

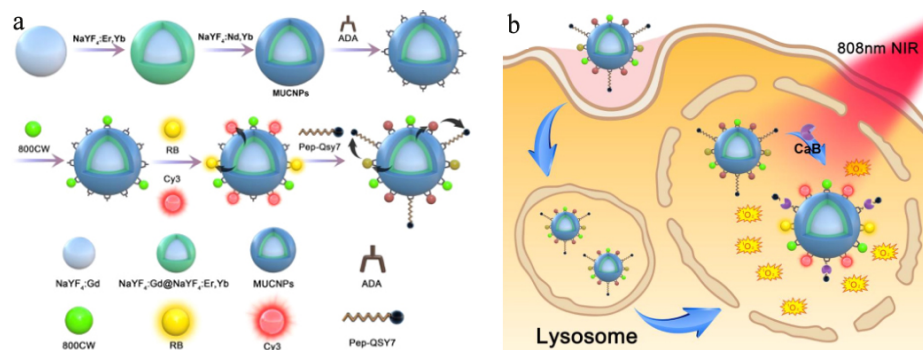


Figure 6. Schematic illustrations of (a) synthesis of the upconversion nanoprobe and (b) Intracellular CaB-Activated PDT with CaB imaging for Therapeutic Effect Prediction, reprinted with permission from ref. [145]. Copyright 2020 American Chemical Society.

Similarly, the Zhang group [146] designed an amplifier with multiple upconversion luminescence, composed of photo-caged DNA nano-combs and upconversion nanoparticles (UCNPs) sensitized with IRDye[®] 800CW, to realize the near-infrared light switch cascade reaction triggered by specific microRNA and accurate photodynamic therapy for early cancer. Under 808 nm light irradiation, the generated ultraviolet light cuts off the “photozipper” to induce the cascade hybridization reaction of the microRNA response. This activates the photosensitizer connected to different hairpins to produce reactive oxygen species (ROS) under the blue light emitted simultaneously, to carry out effective PDT, as shown in Figure 7. The amplifier showed desirable serum stability, excellent controllability of reactive oxygen species generation, high specificity for target cancer, and sensitivity to specific microRNA expression. In vivo and in vitro experiments showed strong inhibition on cell proliferation, strong ability to induce apoptosis of tumor cells, and distinct inhibition of tumor growth.

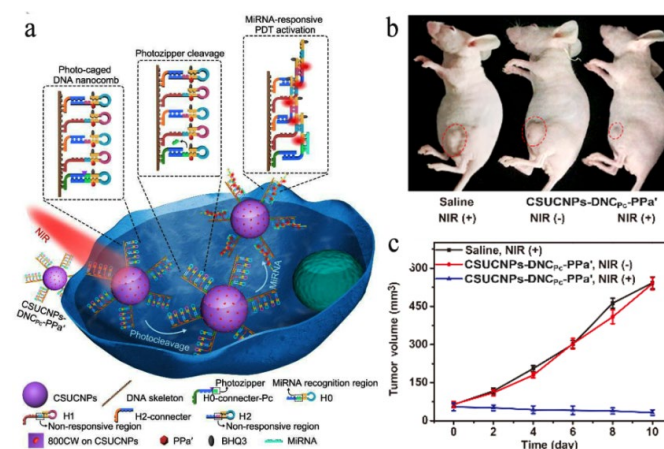


Figure 7. (a) Schematic illustration of NIR photo-switched miRNA amplifier for precise PDT. (b) Representative images at day 10 and (c) tumor volumes of early-stage breast cancer-bearing mice, treated with saline, CSUCNPs-DNC_{Pc}-PPa' and CSUCNPs-DNC_{Pc}-PPa' before and after 808 nm light irradiation at 1 W/cm². Error bars indicate means \pm SD ($n = 5$), reprinted with permission from ref. [146]. Copyright 2020 John Wiley and Sons.

Lin et al. [147] designed a spindle-like UCNPs nanoprobe, coated with a layer of gold nanoparticles to enhance upconversion luminescence (UCL), as shown in Figure 8. The results of biocompatibility, blood routine, bioimaging, and anti-cancer tests showed that it was easier for the spindle-like nanoprobe to enter biological tissues. In addition, the combination of SPS@Au and ZnPc (SPSZ) is a potential candidate for synergistic immune photodynamic therapy (PDT), with enhanced UCL effect and excellent biocompatibility.

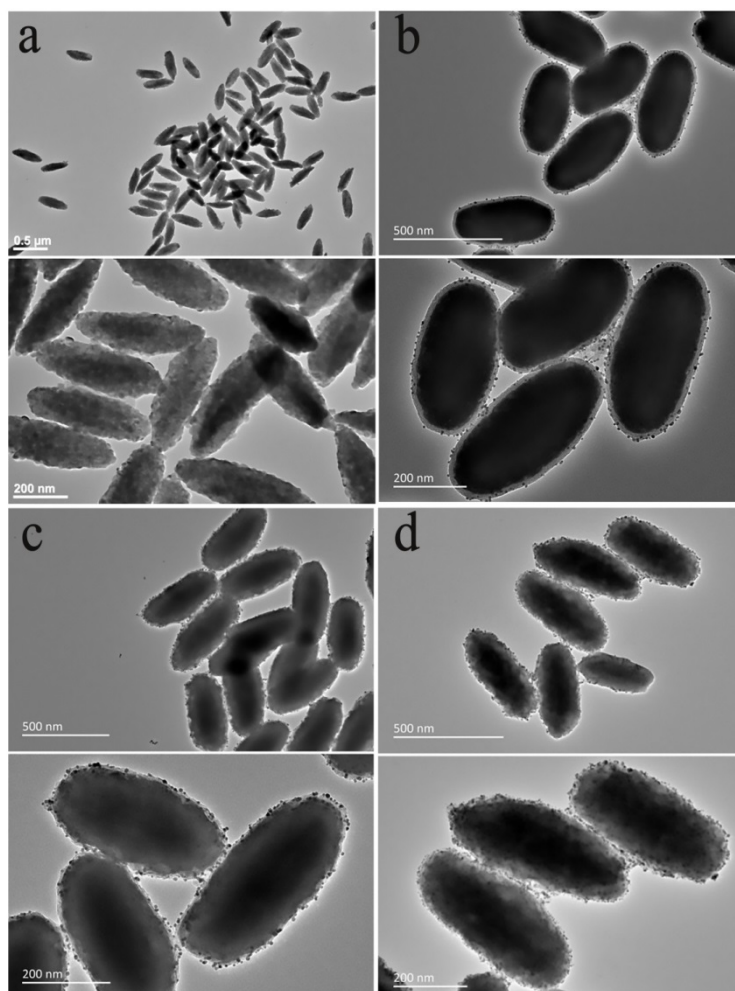


Figure 8. TEM image of (a) spindle precursor and (b) SPS@Au (LBL1) and (c) SPS@Au (LBL2) and (d) SPS@Au (LBL3). Reprinted with permission from ref. [147]. Copyright 2020 American Chemistry Society.

The Li group [148] designed core-satellite metal-organic through electrostatic self-assembly framework@UCNP superstructures, composed of a single metal-organic framework (MOF) NP as the core, and Nd³⁺-sensitized UCNPs as the satellites. In vitro and in vivo experiments show that the double photosensitizer superstructure has a three-mode (magnetic resonance/UCL/ fluorescence) imaging function and excellent anti-tumor effect under the excitation of 808 nm near-infrared light, avoiding overheating caused by laser irradiation. After being exposed to an 808 nm laser for 5 min, the temperature of the irradiated area was lower than 42 °C, and without damage to mice. However, under the same conditions, a 980 nm laser can heat the irradiated area to above 50 °C and severely burn the skin. These findings indicate that 808 nm excitation has a much weaker tissue thermal effect and is more suitable for biological applications.

Sun et al. [149] designed and prepared one kind of lanthanide (Ln³⁺)-doped upconversion nanocomposites with multi-functions, which can not only provide temperature

feedback in PTT process, but also play the photodynamic therapy (PDT) function for the synergistic effect of tumor therapy. Based on NaYF₄:Yb, Er upconversion nanoparticles (UCNPs), mesoporous SiO₂ was modified on the surface combined with photosensitizer Chlorin e6 (Ce6) molecules, which could be excited by red emission of Er³⁺ under the 980 nm laser. Cit-CuS NPs were further linked on the surface of the composite as a photothermal conversion agent, therefore, the temperature of the PTT site can be monitored by recording the ratio of I₅₂₅/I₅₄₅ of green emissions, especially within the physiological range, as shown in Figure 9. Based on the guidance obtained from spectral experiments, they further investigated the dual-modal therapy effect both in vitro and in vivo, respectively, and acquired decent results.

In addition, these rare earth doped nanoparticles also have strong scintillation luminescence that can be used for X-ray induced photodynamic therapy, which is a very hot area, as this new therapy can be used for deep as well as skin cancer treatment [150–163].

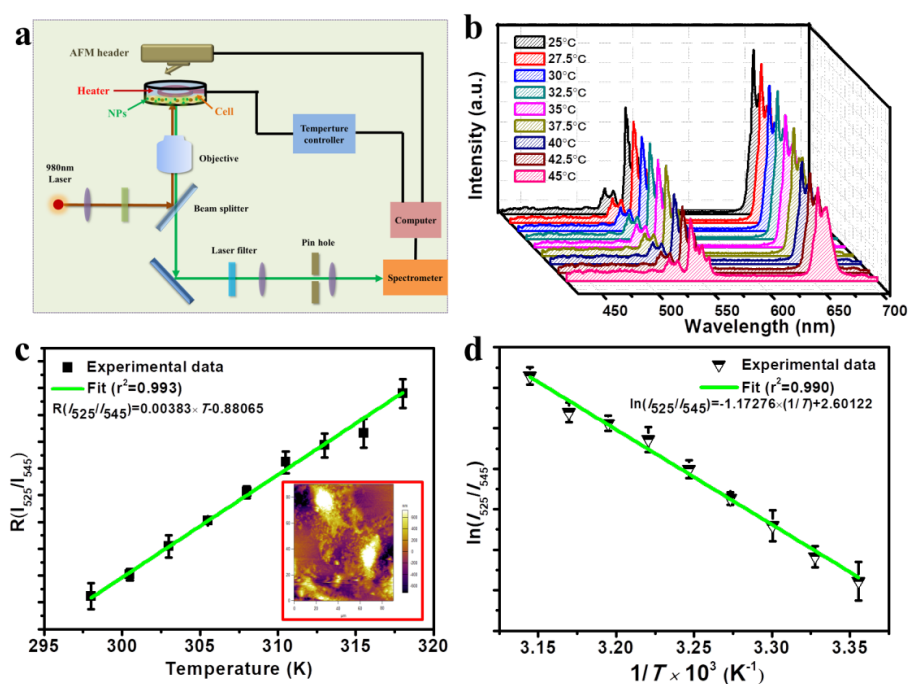


Figure 9. (a) Schematic diagram of the detection of the temperature and emission spectrum of UCNPs-Ce6@mSiO₂-CuS incubated with cells in physiological range; (b) UCL emission spectrum of UCNPs-Ce6@mSiO₂-CuS incubated with cells at different temperatures by external heating. The peaks were normalized at 525 nm; (c) FIR of the green UC emissions for the ²H_{11/2}/⁴S_{3/2} → ⁴I_{15/2} transitions relative to the temperature of UCNPs-Ce6@mSiO₂-CuS incubated with cells. The inset picture is the AFM image of the cell after spectral detection; (d) A plot of ln(I₅₂₅/I₅₄₅) versus 1/T to calibrate the thermometric scale for UCNPs-Ce6@mSiO₂-CuS incubated with cells. Reprinted with permission from ref. [149]. Copyright 2019 Elsevier.

6. Summary and Perspective

Over the last decades, UCNPs have made remarkable advances in the treatment of critical diseases, greatly promoting the application of modern precision medicine in the life system with its enhanced therapeutic effect, high space-time controllability, deep tissue penetration, and minimal invasion. However, despite the remarkable achievements, there are still some challenges of UCNPs. (1) The stability of luminous efficiency after surface modification: in the surface modification, the oil-soluble molecules will be modified to improve biocompatibility. Nevertheless, the dispersing ability of UCNPs in oil and water is different. After surface modification, it is easy to cause fluorescence quenching and reduce the upconversion efficiency. (2) The biological toxicity of UCNPs: many studies have shown that the reasonable optimization of chemical composition, particle size distribution,

and surface modification can significantly improve the biocompatibility of UCNPs, which can be used in biomedical applications. However, there are no tests to evaluate its long-term toxicity, including potential immune response and mutagenic effect. (3) Technical gaps in clinical trials: so far, UCNPs-based phototherapy has not been applied to human beings, mainly due to biosafety or therapeutic effect. There is still a long way to go from laboratory animals to human-level technical standard updates. In summary, UCNPs offer a tremendous opportunity to practice precision medicine. We expect that stable surface modification, low toxicity, and clinical trials will make UCNPs more competitive in the biological field.

Author Contributions: Conceptualization, methodology, Q.L.; validation, formal analysis. and; investigation, resources, visualization; writing—original draft preparation, C.G.; data curation, P.Z. and S.H.; supervision, writing—review and editing, J.W., C.X., T.J., H.T. and W.C.; project administration and instruction, J.W.; funding acquisition, Y.W., D.L. and S.L. All authors have read and agreed to the published version of the manuscript.

Funding: This research was funded by the National Science Foundation of China No. 11904125, the Open Research Subject of Key Laboratory of Dielectric and Electrolyte Functional Material Hebei Province No. HKDE201902, BIGC Project No. 22150121034/026, No. 22150121003/050, No. Eb202105, and JENU No. XZD201802. W. C. would like to thank Solgro Inc. and UT Arlington distinguished award.

Institutional Review Board Statement: Not applicable.

Informed Consent Statement: Not applicable.

Data Availability Statement: The study did not report any data.

Conflicts of Interest: The authors declare no conflict of interest.

References

1. Ouyang, J.; Ripmeester, J.A.; Wu, X.; Kingston, D.; Yu, K.; Joly, A.G.; Chen, W. Upconversion luminescence of colloidal CdS and ZnCdS semiconductor quantum dots. *J. Phys. Chem. C* **2007**, *111*, 16261–16266. [[CrossRef](#)]
2. Porter, J.F., Jr. Fluorescence excitation by the absorption of two consecutive photons. *Phys. Rev. Lett.* **1961**, *7*, 414. [[CrossRef](#)]
3. Yao, J.; Huang, C.; Liu, C.; Yang, M. Upconversion luminescence nanomaterials: A versatile platform for imaging, sensing, and therapy. *Talanta* **2020**, *208*, 120157. [[CrossRef](#)] [[PubMed](#)]
4. Ansari, A.A.; Parchur, A.K.; Thorat, N.D.; Chen, G. New advances in pre-clinical diagnostic imaging perspectives of functionalized upconversion nanoparticle-based nanomedicine. *Coord. Chem. Rev.* **2021**, *440*, 213971. [[CrossRef](#)]
5. Xin, N.; Wei, D.; Zhu, Y.; Yang, M.; Ramakrishna, S.; Lee, O.; Luo, H.; Fan, H. Upconversion nanomaterials: A platform for biosensing, theranostic and photoregulation. *Mater. Today Chem.* **2020**, *17*, 100329. [[CrossRef](#)]
6. Wang, J.; Sheng, T.; Zhu, X.; Li, Q.; Wu, Y.; Zhang, J.; Liu, J.; Zhang, Y. Spectral engineering of lanthanide-doped upconversion nanoparticles and their biosensing applications. *Mater. Chem. Front.* **2021**, *5*, 1743–1770. [[CrossRef](#)]
7. Peltomaa, R.; Benito-Peña, E.; Gorris, H.H.; Moreno-Bondi, M.C. Biosensing based on upconversion nanoparticles for food quality and safety applications. *Analyst* **2021**, *146*, 13–32. [[CrossRef](#)]
8. Freeman, A.J.; Watson, R.E. Theoretical investigation of some magnetic and spectroscopic properties of rare-earth ions. *Phys. Rev.* **1962**, *127*, 2058. [[CrossRef](#)]
9. Yan, C.; Jia, J.; Liao, C.; Wu, S.; Xu, G. Rare earth separation in China. *Tsinghua Sci. Technol.* **2006**, *11*, 241–247. [[CrossRef](#)]
10. Bünzli, J.C.G. Benefiting from the unique properties of lanthanide ions. *Acc. Chem. Res.* **2006**, *39*, 53–61. [[CrossRef](#)]
11. Sun, L.D.; Dong, H.; Zhang, P.Z.; Yan, C.H. Upconversion of rare earth nanomaterials. *Annu. Rev. Phys. Chem.* **2015**, *66*, 619–642. [[CrossRef](#)]
12. Tian, B.; Bravo, A.F.; Najafiaghdam, H.; Torquato, N.A.; Altoe, M.V.P.; Teitelboim, A.; Tajon, C.A.; Tian, Y.; Borys, N.J.; Barnard, E.S.; et al. Low irradiance multiphoton imaging with alloyed lanthanide nanocrystals. *Nat. Commun.* **2018**, *9*, 1–8. [[CrossRef](#)] [[PubMed](#)]
13. Zhan, Q.; Liu, H.; Wang, B.; Wu, Q.; Pu, R.; Zhou, C.; Huang, B.; Peng, X.; Agren, H.; He, S. Achieving high-efficiency emission depletion nanoscopy by employing cross relaxation in upconversion nanoparticles. *Nat. Commun.* **2017**, *8*, 1–11. [[CrossRef](#)] [[PubMed](#)]
14. Qiu, Z.; Shu, J.; Tang, D. Near-infrared-to-ultraviolet light-mediated photoelectrochemical aptasensing platform for cancer biomarker based on core-shell NaYF₄: Yb, Tm@TiO₂ upconversion microrods. *Anal. Chem.* **2018**, *90*, 1021–1028. [[CrossRef](#)] [[PubMed](#)]

15. Zhang, K.; Song, S.; Huang, S.; Yang, L.; Min, Q.; Wu, X.; Lu, F.; Zhu, J.J. Lighting Up MicroRNA in Living Cells by the Disassembly of Lock-Like DNA-Programmed UCNPs-AuNPs through the Target Cycling Amplification Strategy. *Small* **2018**, *14*, 1802292. [[CrossRef](#)]
16. Yao, C.; Wang, P.; Li, X.; Hu, X.; Hou, J.; Wang, L.; Zhang, F. Near-infrared-triggered azobenzene-liposome/upconversion nanoparticle hybrid vesicles for remotely controlled drug delivery to overcome cancer multidrug resistance. *Adv. Mater.* **2016**, *28*, 9341–9348. [[CrossRef](#)]
17. Chen, X.; Tang, Y.; Liu, A.; Zhu, Y.; Gao, D.; Yang, Y.; Sun, J.; Fan, H.; Zhang, X. NIR-to-red upconversion nanoparticles with minimized heating effect for synchronous multidrug resistance tumor imaging and therapy. *ACS Appl. Mater. Interfaces* **2018**, *10*, 14378–14388. [[CrossRef](#)]
18. Chen, X.; Sun, J.; Zhao, H.; Yang, K.; Zhu, Y.; Luo, H.; Yu, K.; Fan, K.; Zhang, X. Theranostic system based on NaY(Mn)F₄: Yb/Er upconversion nanoparticles with multi-drug resistance reversing ability. *J. Mater. Chem. B* **2018**, *6*, 3586–3599. [[CrossRef](#)]
19. Yao, J.; Yang, M.; Duan, Y. Chemistry, biology, and medicine of fluorescent nanomaterials and related systems: New insights into biosensing, bioimaging, genomics, diagnostics, and therapy. *Chem. Rev.* **2014**, *114*, 6130–6178. [[CrossRef](#)]
20. Chen, W.; Joly, A.G.; McCready, D.E. Upconversion luminescence from CdSe nanoparticles. *J. Chem. Phys.* **2005**, *122*, 224708. [[CrossRef](#)]
21. Joly, A.G.; Chen, W.; McCready, D.E.; Malm, J.O.; Bovin, J.O. Upconversion luminescence of CdTe nanoparticles. *Phys. Rev. B* **2005**, *71*, 165304. [[CrossRef](#)]
22. Shen, J.; Sun, L.D.; Yan, C.H. Luminescent rare earth nanomaterials for bioprobe applications. *Dalton Trans.* **2008**, 5687–5697. [[CrossRef](#)]
23. Wang, F.; Banerjee, D.; Liu, Y.; Chen, X.; Liu, X. Upconversion nanoparticles in biological labeling, imaging, and therapy. *Analyst* **2010**, *135*, 1839–1854. [[CrossRef](#)] [[PubMed](#)]
24. Zhou, J.; Liu, Z.; Li, F. Upconversion nanophosphors for small-animal imaging. *Chem. Soc. Rev.* **2012**, *41*, 1323–1349. [[CrossRef](#)] [[PubMed](#)]
25. Hampl, J.; Hall, M.; Mufti, N.A.; Yung-mae, M.Y.; MacQueen, D.B.; Wright, W.H.; Cooper, D.E. Upconverting phosphor reporters in immunochromatographic assays. *Anal. Biochem.* **2001**, *288*, 176–187. [[CrossRef](#)] [[PubMed](#)]
26. Van De Rijke, F.; Zijlmans, H.; Li, S.; Vail, T.; Raap, A.K.; Niedbala, R.S.; Tanke, H.J. Up-converting phosphor reporters for nucleic acid microarrays. *Nat. Biotechnol.* **2001**, *19*, 273–276. [[CrossRef](#)]
27. Zhang, P.; Rogelj, S.; Nguyen, K.; Wheeler, D. Design of a highly sensitive and specific nucleotide sensor based on photon upconverting particles. *J. Am. Chem. Soc.* **2006**, *128*, 12410–12411. [[CrossRef](#)]
28. Chatterjee, D.K.; Gnanasammandhan, M.K.; Zhang, Y. Small upconverting fluorescent nanoparticles for biomedical applications. *Small* **2010**, *6*, 2781–2795. [[CrossRef](#)]
29. Cheng, L.; Wang, C.; Liu, Z. Upconversion nanoparticles and their composite nanostructures for biomedical imaging and cancer therapy. *Nanoscale* **2013**, *5*, 23–37. [[CrossRef](#)]
30. Gu, Z.; Yan, L.; Tian, G.; Li, S.; Chai, Z.; Zhao, Y. Recent advances in design and fabrication of upconversion nanoparticles and their safe theranostic applications. *Adv. Mater.* **2013**, *25*, 3758–3779. [[CrossRef](#)]
31. Wilson, B.C.; Patterson, M.S. The physics, biophysics and technology of photodynamic therapy. *Phys. Med. Biol.* **2008**, *53*, R61. [[CrossRef](#)]
32. Li, S.; Cui, S.; Yin, D.; Zhu, Q.; Ma, Y.; Qian, Z.; Gu, Y. Dual antibacterial activities of a chitosan-modified upconversion photodynamic therapy system against drug-resistant bacteria in deep tissue. *Nanoscale* **2017**, *9*, 3912–3924. [[CrossRef](#)] [[PubMed](#)]
33. Lucky, S.S.; Idris, N.M.; Huang, K.; Kim, J.; Li, Z.; Thong, P.S.P.; Xu, R.; Soo, K.C.; Zhang, Y. In vivo biocompatibility, biodistribution and therapeutic efficiency of titania coated upconversion nanoparticles for photodynamic therapy of solid oral cancers. *Theranostics* **2016**, *6*, 1844–1865. [[CrossRef](#)] [[PubMed](#)]
34. Wang, D.; Liu, B.; Quan, Z.; Li, C.; Hou, Z.; Xing, B.; Lin, J. New advances on the marrying of UCNPs and photothermal agents for imaging-guided diagnosis and the therapy of tumors. *J. Mater. Chem. B* **2017**, *5*, 2209–2230. [[CrossRef](#)] [[PubMed](#)]
35. Chen, W.; Joly, A.G.; Malm, J.O.; Bovin, J.O. Upconversion luminescence of Eu³⁺ and Mn²⁺ in ZnS: Mn²⁺, Eu³⁺ codoped nanoparticles. *J. Appl. Phys.* **2004**, *95*, 667–672. [[CrossRef](#)]
36. Chen, W.; Joly, A.G.; Zhang, J.Z. Up-conversion luminescence of Mn²⁺ in ZnS:Mn²⁺ nanoparticles. *Phys. Rev. B* **2001**, *64*, 041202. [[CrossRef](#)]
37. Bruschini, C.; Homulle, H.; Antolovic, I.M.; Burri, S.; Charbon, E. Single-photon avalanche diode imagers in biophotonics: Review and outlook. *Light Sci. Appl.* **2019**, *8*, 1–28. [[CrossRef](#)] [[PubMed](#)]
38. Li, Z.; Ding, X.; Cong, H.; Wang, S.; Yu, B.; Shen, Y. Recent advances on inorganic lanthanide-doped NIR-II fluorescence nanoprobes for bioapplication. *J. Lumin.* **2020**, *228*, 117627. [[CrossRef](#)]
39. Auzel, F. Upconversion and anti-stokes processes with f and d ions in solids. *Chem. Rev.* **2004**, *104*, 139–174. [[CrossRef](#)]
40. Sun, Y.; Chen, Y.; Tian, L.; Yu, Y.; Kong, X.; Zhao, J.; Zhang, H. Controlled synthesis and morphology dependent upconversion luminescence of NaYF₄: Yb, Er nanocrystals. *Nanotechnology* **2007**, *18*, 275609. [[CrossRef](#)]
41. Wang, L.; Li, Y. Green upconversion nanocrystals for DNA detection. *Chem. Commun.* **2006**, *131*, 2557–2559. [[CrossRef](#)] [[PubMed](#)]
42. Wang, L.; Li, Y. Na(Y_{1.5}Na_{0.5})F₆ single-crystal nanorods as multicolor luminescent materials. *Nano Lett.* **2006**, *6*, 1645–1649. [[CrossRef](#)] [[PubMed](#)]

43. De la Rosa, E.; Salas, P.; Desirena, H.; Angeles, C.; Rodriguez, R.A. Strong green upconversion emission in ZrO_2 : Yb^{3+} - Ho^{3+} nanocrystals. *Appl. Phys. Lett.* **2005**, *87*, 241912. [[CrossRef](#)]
44. Wang, G.; Peng, Q.; Li, Y. Upconversion luminescence of monodisperse CaF_2 : Yb^{3+} / Er^{3+} nanocrystals. *J. Am. Chem. Soc.* **2009**, *131*, 14200–14201. [[CrossRef](#)] [[PubMed](#)]
45. Wang, F.; Liu, X. Upconversion multicolor fine-tuning: Visible to near-infrared emission from lanthanide-doped NaYF_4 nanoparticles. *J. Am. Chem. Soc.* **2008**, *130*, 5642–5643. [[CrossRef](#)]
46. Chen, G.; Ohulchanskyy, T.Y.; Kachynski, A.; Ågren, H.; Prasad, P.N. Intense visible and near-infrared upconversion photoluminescence in colloidal LiYF_4 : Er^{3+} nanocrystals under excitation at 1490 nm. *ACS Nano* **2011**, *5*, 4981–4986. [[CrossRef](#)]
47. Chen, D.; Lei, L.; Yang, A.; Wang, Z.; Wang, Y. Ultra-broadband near-infrared excitable upconversion core/shell nanocrystals. *Chem. Commun.* **2012**, *48*, 5898–5900. [[CrossRef](#)]
48. Chen, G.; Ohulchanskyy, T.Y.; Liu, S.; Law, W.C.; Wu, F.; Swihart, M.T.; Ågren, H.; Prasad, P.N. Core/shell NaGdF_4 : Nd^{3+} / NaGdF_4 nanocrystals with efficient near-infrared to near-infrared downconversion photoluminescence for bioimaging applications. *ACS Nano* **2012**, *6*, 2969–2977. [[CrossRef](#)]
49. Rui-Rong, W.; Guo, J.; Zhi-Heng, F.; Wei, W.; Xiang-Fu, M.; Zhi-Yong, X.; Fan, Z. Broadband time-resolved elliptical crystal spectrometer for X-ray spectroscopic measurements in laser-produced plasmas. *Chin. Phys. B* **2014**, *23*, 113201.
50. Rakov, N.; Maciel, G.S.; Sundheimer, M.L.; de S. Menezes, L.; Gomes, A.S.L.; Messaddeq, Y.; Cassanjes, F.C.; Poirier, G.; Ribeiro, S.J.L. Blue upconversion enhancement by a factor of 200 in Tm^{3+} -doped tellurite glass by codoping with Nd^{3+} ions. *J. Appl. Phys.* **2002**, *92*, 6337–6339. [[CrossRef](#)]
51. Wang, L.; Qin, W.; Liu, Z.; Zhao, D.; Qin, G.; Di, W.; He, C. Improved 800 nm emission of Tm^{3+} sensitized by Yb^{3+} and Ho^{3+} in β - NaYF_4 nanocrystals under 980 nm excitation. *Opt. Express* **2012**, *20*, 7602–7607. [[CrossRef](#)]
52. Liang, H.; Chen, G.; Li, L.; Liu, Y.; Qin, F.; Zhang, Z. Upconversion luminescence in Yb^{3+} / Tb^{3+} -codoped monodisperse NaYF_4 nanocrystals. *Opt. Commun.* **2009**, *282*, 3028–3031. [[CrossRef](#)]
53. Dwivedi, Y.; Thakur, S.N.; Rai, S.B. Study of frequency upconversion in Yb^{3+} / Eu^{3+} by cooperative energy transfer in oxyfluoroborate glass matrix. *Appl. Phys. B* **2007**, *89*, 45–51. [[CrossRef](#)]
54. Uvarova, T.V.; Kiiko, V.V. Up-conversion multiwave (White) luminescence in the visible spectral range under excitation by IR laser diodes in the active BaY_2F_8 : Yb^{3+} , Pr^{3+} medium. *Opt. Spectrosc.* **2011**, *111*, 273–276.
55. Xu, B.; Song, C.; Huang, R.; Song, J.; Lin, Z.; Song, J.; Liu, J. Luminescence properties related to energy transfer process and cross relaxation process of Y_2O_3 : Yb^{3+} / Er^{3+} thin films doped with K^+ ion. *Opt. Mater.* **2021**, *118*, 111290. [[CrossRef](#)]
56. Ouertani, G.; Ferhi, M.; Horchani-Naifer, K.; Ferid, M. Effect of Sm^{3+} concentration and excitation wavelength on spectroscopic properties of GdPO_4 : Sm^{3+} phosphor. *J. Alloys Compd.* **2021**, *885*, 161178. [[CrossRef](#)]
57. Zheng, B.; Hong, J.; Chen, B.; Chen, Y.; Lin, R.; Huang, C.; Zhang, C.; Wang, J.; Lin, L.; Zheng, Z. Quantum cutting properties in KYF_4 : Tb^{3+} , Yb^{3+} phosphors: Judd-Ofelt analysis, rate equation models and dynamic processes. *Results Phys.* **2021**, *28*, 104595. [[CrossRef](#)]
58. Kumar, A.; Bahadur, A. Intense green upconversion emission by photon avalanche process from Er^{3+} / Yb^{3+} -co-doped $\text{NaBi}(\text{WO}_4)_2$ phosphor. *J. Alloys Compd.* **2021**, *857*, 158196. [[CrossRef](#)]
59. Liu, T.; Song, Y.; Wang, S.; Li, Y.; Yin, Z.; Qiu, J.; Yang, Z.; Song, Z. Two distinct simultaneous NIR looping behaviours of Er^{3+} singly doped BiOBr : The underlying nature of the Er^{3+} ion photon avalanche emission induced by a layered structure. *J. Alloys Compd.* **2019**, *779*, 440–449. [[CrossRef](#)]
60. Wang, F.; Liu, X. Recent advances in the chemistry of lanthanide-doped upconversion nanocrystals. *Chem. Soc. Rev.* **2009**, *38*, 976–989. [[CrossRef](#)]
61. Chen, G.; Qiu, H.; Prasad, P.N.; Chen, X. Upconversion nanoparticles: Design, nanochemistry, and applications in theranostics. *Chem. Rev.* **2014**, *114*, 5161–5214. [[CrossRef](#)] [[PubMed](#)]
62. Liu, Y.; Tu, D.; Zhu, H.; Chen, X. Lanthanide-doped luminescent nanoprobes: Controlled synthesis, optical spectroscopy, and bioapplications. *Chem. Soc. Rev.* **2013**, *42*, 6924–6958. [[CrossRef](#)] [[PubMed](#)]
63. Feng, W.; Han, C.; Li, F. Upconversion-nanophosphor-based functional nanocomposites. *Adv. Mater.* **2013**, *25*, 5287–5303. [[CrossRef](#)]
64. Zhang, Y.W.; Sun, X.; Si, R.; You, L.P.; Yan, C.H. Single-crystalline and monodisperse LaF_3 triangular nanoplates from a single-source precursor. *J. Am. Chem. Soc.* **2005**, *127*, 3260–3261. [[CrossRef](#)] [[PubMed](#)]
65. Mai, H.X.; Zhang, Y.W.; Si, R.; Yan, Z.G.; Sun, L.D.; You, L.P.; Yan, C.H. High-quality sodium rare-earth fluoride nanocrystals: Controlled synthesis and optical properties. *J. Am. Chem. Soc.* **2006**, *128*, 6426–6436. [[CrossRef](#)]
66. Du, Y.P.; Sun, X.; Zhang, Y.W.; Yan, Z.G.; Sun, L.D.; Yan, C.H. Uniform alkaline earth fluoride nanocrystals with diverse shapes grown from thermolysis of metal trifluoroacetates in hot surfactant solutions. *Cryst. Growth Des.* **2009**, *9*, 2013–2019. [[CrossRef](#)]
67. Mahalingam, V.; Vetrone, F.; Naccache, R.; Speghini, A.; Capobianco, J.A. Colloidal Tm^{3+} / Yb^{3+} -doped LiYF_4 nanocrystals: Multiple luminescence spanning the UV to NIR regions via low-energy excitation. *Adv. Mater.* **2009**, *21*, 4025–4028. [[CrossRef](#)]
68. Vetrone, F.; Naccache, R.; Mahalingam, V.; Morgan, C.G.; Capobianco, J.A. The active-core/active-shell approach: A strategy to enhance the upconversion luminescence in lanthanide-doped nanoparticles. *Adv. Funct. Mater.* **2009**, *19*, 2924–2929. [[CrossRef](#)]
69. Yang, D.; Li, C.; Li, G.; Shang, M.; Kang, X.; Lin, J. Colloidal synthesis and remarkable enhancement of the upconversion luminescence of BaGdF_5 : Yb^{3+} / Er^{3+} nanoparticles by active-shell modification. *J. Mater. Chem.* **2011**, *21*, 5923–5927. [[CrossRef](#)]

70. Mahalingam, V.; Vetrone, F.; Naccache, R.; Speghini, A.; Capobianco, J.A. Structural and optical investigation of colloidal $\text{Ln}^{3+}/\text{Yb}^{3+}$ co-doped KY_3F_{10} nanocrystals. *J. Mater. Chem.* **2009**, *19*, 3149–3152. [[CrossRef](#)]
71. Wang, H.; Nakamura, H.; Uehara, M.; Yamaguchi, Y.; Miyazaki, M.; Maeda, H. Highly luminescent CdSe/ZnS nanocrystals synthesized using a single-molecular ZnS source in a microfluidic reactor. *Adv. Funct. Mater.* **2005**, *15*, 603–608. [[CrossRef](#)]
72. Sun, X.; Zhang, Y.W.; Du, Y.P.; Yan, Z.G.; Si, R.; You, L.P.; Yan, C.H. From trifluoroacetate complex precursors to monodisperse rare-earth fluoride and oxyfluoride nanocrystals with diverse shapes through controlled fluorination in solution phase. *Chem. A Eur. J.* **2007**, *13*, 2320–2332. [[CrossRef](#)]
73. Chen, D.; Huang, P.; Yu, Y.; Huang, F.; Yang, A.; Wang, Y. Dopant-induced phase transition: A new strategy of synthesizing hexagonal upconversion NaYF_4 at low temperature. *Chem. Commun.* **2011**, *47*, 5801–5803. [[CrossRef](#)] [[PubMed](#)]
74. Chen, D.; Yu, Y.; Huang, F.; Huang, P.; Yang, A.; Wang, Y. Modifying the size and shape of monodisperse bifunctional alkaline-earth fluoride nanocrystals through lanthanide doping. *J. Am. Chem. Soc.* **2010**, *132*, 9976–9978. [[CrossRef](#)] [[PubMed](#)]
75. Wang, F.; Chatterjee, D.K.; Li, Z.; Zhang, Y.; Fan, X.; Wang, M. Synthesis of polyethylenimine/ NaYF_4 nanoparticles with upconversion fluorescence. *Nanotechnology* **2006**, *17*, 5786. [[CrossRef](#)]
76. Wang, L.; Li, P.; Li, Y. Down-and up-conversion luminescent nanorods. *Adv. Mater.* **2007**, *19*, 3304–3307. [[CrossRef](#)]
77. Zeng, S.; Xiao, J.; Yang, Q.; Hao, J. Bi-functional NaLuF_4 : $\text{Gd}^{3+}/\text{Yb}^{3+}/\text{Tm}^{3+}$ nanocrystals: Structure controlled synthesis, near-infrared upconversion emission and tunable magnetic properties. *J. Mater. Chem.* **2012**, *22*, 9870–9874. [[CrossRef](#)]
78. Zeng, J.H.; Xie, T.; Li, Z.H.; Li, Y. Monodispersed nanocrystalline fluoroperovskite up-conversion phosphors. *Cryst. Growth Des.* **2007**, *7*, 2774–2777. [[CrossRef](#)]
79. Zeng, S.; Tsang, M.K.; Chan, C.F.; Wong, K.L.; Hao, J. PEG modified BaGdF_5 : Yb/Er nanoprobes for multi-modal upconversion fluorescent, in vivo X-ray computed tomography and biomagnetic imaging. *Biomaterials* **2012**, *33*, 9232–9238. [[CrossRef](#)]
80. Vetrone, F.; Boyer, J.C.; Capobianco, J.A.; Speghini, A.; Bettinelli, M. Significance of Yb^{3+} concentration on the upconversion mechanisms in codoped Y_2O_3 : Er^{3+} , Yb^{3+} nanocrystals. *J. Appl. Phys.* **2004**, *96*, 661–667. [[CrossRef](#)]
81. Shang, M.; Li, G.; Kang, X.; Yang, D.; Geng, D.; Peng, C.; Cheng, Z.; Lian, H.; Lin, J. LaOF: Eu^{3+} nanocrystals: Hydrothermal synthesis, white and color-tuning emission properties. *Dalton Trans.* **2012**, *41*, 5571–5580. [[CrossRef](#)] [[PubMed](#)]
82. Heer, S.; Lehmann, O.; Haase, M.; Gudel, H.U. Blue, green, and red upconversion emission from lanthanide-doped LuPO_4 and YbPO_4 nanocrystals in a transparent colloidal solution. *Angew. Chem. Int. Ed.* **2003**, *42*, 3179–3182. [[CrossRef](#)]
83. Schäfer, H.; Ptacek, P.; Eickmeier, H.; Haase, M. Synthesis of Hexagonal Yb^{3+} , Er^{3+} -Doped NaYF_4 Nanocrystals at Low Temperature. *Adv. Funct. Mater.* **2009**, *19*, 3091–3097. [[CrossRef](#)]
84. Ptacek, P.; Schäfer, H.; Kömpe, K.; Haase, M. Crystal Phase Control of Luminescing α - NaGdF_4 : Eu^{3+} and β - NaGdF_4 : Eu^{3+} Nanocrystals. *Adv. Funct. Mater.* **2007**, *17*, 3843–3848. [[CrossRef](#)]
85. Gai, S.; Yang, G.; Li, X.; Li, C.; Dai, Y.; He, F.; Yang, P. Facile synthesis and up-conversion properties of monodisperse rare earth fluoride nanocrystals. *Dalton Trans.* **2012**, *41*, 11716–11724. [[CrossRef](#)]
86. Yang, T.; Sun, Y.; Liu, Q.; Feng, W.; Yang, P.; Li, F. Cubic sub-20 nm NaLuF_4 -based upconversion nanophosphors for high-contrast bioimaging in different animal species. *Biomaterials* **2012**, *33*, 3733–3742. [[CrossRef](#)] [[PubMed](#)]
87. Wong, H.T.; Vetrone, F.; Naccache, R.; Chan, H.L.W.; Hao, J.; Capobianco, J.A. Water dispersible ultra-small multifunctional KGdF_4 : Tm^{3+} , Yb^{3+} nanoparticles with near-infrared to near-infrared upconversion. *J. Mater. Chem.* **2011**, *21*, 16589–16596. [[CrossRef](#)]
88. Dai, Y.; Zhang, C.; Cheng, Z.; Li, C.; Kang, X.; Yang, D.; Lin, J. pH-responsive drug delivery system based on luminescent CaF_2 : $\text{Ce}^{3+}/\text{Tb}^{3+}$ -poly (acrylic acid) hybrid microspheres. *Biomaterials* **2012**, *33*, 2583–2592. [[CrossRef](#)] [[PubMed](#)]
89. Yi, G.S.; Chow, G.M. Colloidal LaF_3 : Yb, Er, LaF_3 : Yb, Ho and LaF_3 : Yb, Tm nanocrystals with multicolor upconversion fluorescence. *J. Mater. Chem.* **2005**, *15*, 4460–4464. [[CrossRef](#)]
90. Teng, X.; Zhu, Y.; Wei, W.; Wang, S.; Huang, J.; Naccache, R.; Hu, W.; Tok, A.; Han, Y.; Zhang, Q.; et al. Lanthanide-doped $\text{Na}_x\text{ScF}_{3+x}$ nanocrystals: Crystal structure evolution and multicolor tuning. *J. Am. Chem. Soc.* **2012**, *134*, 8340–8343. [[CrossRef](#)]
91. Liu, H.; Liu, M.; Wang, K.; Wang, B.; Jian, X.; Bai, G.; Zhang, Y. Efficient upconversion emission and high-sensitivity thermometry of BaIn_2O_4 : $\text{Yb}^{3+}/\text{Tm}^{3+}/\text{RE}^{3+}$ ($\text{RE} = \text{Er}^{3+}$, Ho^{3+}) phosphor. *Dalton Trans.* **2021**, *50*, 12107–12117. [[CrossRef](#)] [[PubMed](#)]
92. Lim, C.S.; Aleksandrovsky, A.S.; Atuchin, V.V.; Molokeyev, M.S.; Oreshonkov, A.S. Microwave sol-gel synthesis, microstructural and spectroscopic properties of scheelite-type ternary molybdate upconversion phosphor $\text{NaPbLa}(\text{MoO}_4)_3$: $\text{Er}^{3+}/\text{Yb}^{3+}$. *J. Alloys Compd.* **2020**, *826*, 152095. [[CrossRef](#)]
93. Wang, G.; Jia, G.; Wang, J.; Kong, H.; Lu, Y.; Zhang, C. Novel rare earth activator ions-doped perovskite-type $\text{La}_4\text{Ti}_3\text{O}_{12}$ phosphors: Facile synthesis, structure, multicolor emissions, and potential applications. *J. Alloys Compd.* **2021**, *877*, 160217. [[CrossRef](#)]
94. Zhang, Y.; Jia, H.; He, X.; Zheng, Y.; Bai, R.; Liu, H. Investigation of enhancing upconversion and temperature sensing performance of Er^{3+} , Yb^{3+} , Bi^{3+} codoped Gd_2O_3 phosphor. *J. Lumin.* **2021**, *236*, 118111. [[CrossRef](#)]
95. Singh, P.; Jain, N.; Tiwari, A.K.; Shukla, S.; Baranwal, V.; Singh, J.; Pandey, A.C. Near-infrared light-mediated Er^{3+} and Yb^{3+} co-doped CaTi_4O_9 for optical temperature sensing behavior. *J. Lumin.* **2021**, *233*, 117737. [[CrossRef](#)]
96. Mokoena, P.P.; Oluwole, D.O.; Nyokong, T.; Swart, H.C.; Ntwaeaborwa, O.M. Enhanced upconversion emission of Er^{3+} - Yb^{3+} co-doped $\text{Ba}_5(\text{PO}_4)_3\text{OH}$ powder phosphor for application in photodynamic therapy. *Sens. Actuators A Phys.* **2021**, *331*, 113014. [[CrossRef](#)]
97. Khajuria, P.; Bedyal, A.K.; Manhas, M.; Swart, H.C.; Durani, F.; Kumar, V. Spectral, surface and thermometric investigations of upconverting $\text{Er}^{3+}/\text{Yb}^{3+}$ co-doped $\text{Na}_3\text{Y}(\text{PO}_4)_2$ phosphor. *J. Alloys Compd.* **2021**, *877*, 160327. [[CrossRef](#)]

98. Oliva, J.; Chávez, D.; González-Galván, A.; Viesca-Villanueva, E.; Díaz-Torres, L.A.; Fraga, J.; García, C.R. Tunable green/yellow upconversion emission and enhancement of the NIR luminescence in BaLaAlO₄: Er³⁺ phosphors by codoping with Yb³⁺ ions. *Optik* **2021**, *241*, 167011. [[CrossRef](#)]
99. Li, M.; Xie, T.; Tu, X.; Xu, J.; Lei, R.; Zhao, S.; Xu, S. Effects of doping concentration and excitation density on optical thermometric behaviors in Ho³⁺/Yb³⁺ co-doped ZrO₂ upconversion nanocrystals. *Opt. Mater.* **2019**, *97*, 109478. [[CrossRef](#)]
100. Siai, A.; Ajili, L.; Horchani-Naifer, K.; Ferid, M. Tm³⁺ Modifying Er³⁺ Red Emission and Dielectric Properties of Tm³⁺-Doped LaErO₃ Perovskite. *J. Electron. Mater.* **2020**, *49*, 3096–3105. [[CrossRef](#)]
101. Boyer, J.C.; Vetrone, F.; Cuccia, L.A.; Capobianco, J.A. Synthesis of colloidal upconverting NaYF₄ nanocrystals doped with Er³⁺, Yb³⁺ and Tm³⁺, Yb³⁺ via thermal decomposition of lanthanide trifluoroacetate precursors. *J. Am. Chem. Soc.* **2006**, *128*, 7444–7445. [[CrossRef](#)]
102. Boyer, J.C.; Cuccia, L.A.; Capobianco, J.A. Synthesis of colloidal upconverting NaYF₄: Er³⁺/Yb³⁺ and Tm³⁺/Yb³⁺ monodisperse nanocrystals. *Nano Lett.* **2007**, *7*, 847–852. [[CrossRef](#)]
103. Ye, X.; Collins, J.E.; Kang, Y.; Chen, J.; Chen, D.T.; Yodh, A.G.; Murray, C.B. Morphologically controlled synthesis of colloidal upconversion nanophosphors and their shape-directed self-assembly. *Proc. Natl. Acad. Sci. USA* **2010**, *107*, 22430–22435. [[CrossRef](#)]
104. Maurya, S.K.; da Silva, J.E.; Mohan, M.; Poddar, R.; Kumar, K. Assessment of colloidal NaGdF₄: Er³⁺/Yb³⁺ upconversion phosphor as contrast enhancer for optical coherence tomography. *J. Alloys Compd.* **2021**, *865*, 158737. [[CrossRef](#)]
105. Pu, Y.; Lin, L.; Wang, D.; Wang, J.X.; Qian, J.; Chen, J.F. Green synthesis of highly dispersed ytterbium and thulium co-doped sodium yttrium fluoride microphosphors for in situ light upconversion from near-infrared to blue in animals. *J. Colloid Interface Sci.* **2018**, *511*, 243–250. [[CrossRef](#)] [[PubMed](#)]
106. Kang, X.J.; Dai, Y.L.; Ma, P.A.; Yang, D.M.; Li, C.X.; Hou, Z.Y.; Cheng, Z.Y.; Lin, J. Poly (acrylic acid)-modified Fe₃O₄ microspheres for magnetic-targeted and ph-triggered anticancer drug delivery. *Chem. A Eur. J.* **2012**, *18*, 15676–15682. [[CrossRef](#)] [[PubMed](#)]
107. Zeng, J.H.; Su, J.; Li, Z.H.; Yan, R.X.; Li, Y.D. Synthesis and upconversion luminescence of hexagonal-phase NaYF₄: Yb, Er³⁺ phosphors of controlled size and morphology. *Adv. Mater.* **2005**, *17*, 2119–2123.
108. Qiu, H.; Chen, G.; Sun, L.; Hao, S.; Han, G.; Yang, C. Ethylenediaminetetraacetic acid (EDTA)-controlled synthesis of multicolor lanthanide doped BaYF₅ upconversion nanocrystals. *J. Mater. Chem.* **2011**, *21*, 17202–17208. [[CrossRef](#)]
109. Yang, X.; Xiao, Q.; Niu, C.; Jin, N.; Ouyang, J.; Xiao, X.; He, D. Multifunctional core-shell upconversion nanoparticles for targeted tumor cells induced by near-infrared light. *J. Mater. Chem. B* **2013**, *1*, 2757–2763. [[CrossRef](#)] [[PubMed](#)]
110. Zhang, F.; Wan, Y.; Yu, T.; Zhang, F.; Shi, Y.; Xie, S.; Li, Y.; Xu, L.; Tu, B.; Zhao, D. Uniform nanostructured arrays of sodium rare-earth fluorides for highly efficient multicolor upconversion luminescence. *Angew. Chem.* **2007**, *119*, 8122–8125. [[CrossRef](#)]
111. Wang, F.; Han, Y.; Lim, C.S.; Lu, Y.; Wang, J.; Xu, J.; Chen, H.; Zhang, C.; Hong, M.; Liu, X. Simultaneous phase and size control of upconversion nanocrystals through lanthanide doping. *Nature* **2010**, *463*, 1061–1065. [[CrossRef](#)]
112. Wang, X.; Zhuang, J.; Peng, Q.; Li, Y. A general strategy for nanocrystal synthesis. *Nature* **2005**, *437*, 121–124. [[CrossRef](#)]
113. Stouwdam, J.W.; van Veggel, F.C.J.M. Near-infrared emission of redispersible Er³⁺, Nd³⁺, and Ho³⁺ doped LaF₃ nanoparticles. *Nano Lett.* **2002**, *2*, 733–737. [[CrossRef](#)]
114. Yi, G.; Lu, H.; Zhao, S.; Ge, Y.; Yang, W.; Chen, D.; Guo, L.H. Synthesis, characterization, and biological application of size-controlled nanocrystalline NaYF₄: Yb, Er infrared-to-visible up-conversion phosphors. *Nano Lett.* **2004**, *4*, 2191–2196. [[CrossRef](#)]
115. Patra, A.; Friend, C.S.; Kapoor, R.; Prasad, P.N. Upconversion in Er³⁺: ZrO₂ nanocrystals. *J. Phys. Chem. B* **2002**, *106*, 1909–1912. [[CrossRef](#)]
116. Venkatramu, V.; Falcomer, D.; Speghini, A.; Bettinelli, M.; Jayasankar, C.K. Synthesis and luminescence properties of Er³⁺-doped Lu₃Ga₅O₁₂ nanocrystals. *J. Lumin.* **2008**, *128*, 811–813. [[CrossRef](#)]
117. Shang, H.; Zhang, X.; Xu, J.; Han, Y. Effects of preparation methods on the activity of CuO/CeO₂ catalysts for CO oxidation. *Front. Chem. Sci. Eng.* **2017**, *11*, 603–612. [[CrossRef](#)]
118. Park, H.; Yoo, G.Y.; Kim, M.S.; Kim, K.; Lee, C.; Park, S.; Kim, W. Thin film fabrication of upconversion lanthanide-doped NaYF₄ by a sol-gel method and soft lithographical nanopatterning. *J. Alloys Compd.* **2017**, *728*, 927–935. [[CrossRef](#)]
119. Liang, Z.; Wang, X.; Zhu, W.; Zhang, P.; Yang, Y.; Sun, C.; Zhang, J.; Wang, X.; Xu, Z.; Zhao, Y.; et al. Upconversion nanocrystals mediated lateral-flow nanoplatfrom for in vitro detection. *ACS Appl. Mater. Interfaces* **2017**, *9*, 3497–3504. [[CrossRef](#)] [[PubMed](#)]
120. Mahalingam, V.; Mangiarini, F.; Vetrone, F.; Venkatramu, V.; Bettinelli, M.; Speghini, A.; Capobianco, J.A. Bright white upconversion emission from Tm³⁺/Yb³⁺/Er³⁺-doped Lu₃Ga₅O₁₂ nanocrystals. *J. Phys. Chem. C* **2008**, *112*, 17745–17749. [[CrossRef](#)]
121. Wen, T.; Zhou, Y.; Guo, Y.; Zhao, C.; Yang, B.; Wang, Y. Color-tunable and single-band red upconversion luminescence from rare-earth doped Vernier phase ytterbium oxyfluoride nanoparticles. *J. Mater. Chem. C* **2016**, *4*, 684–690. [[CrossRef](#)]
122. Xu, L.; Yu, Y.; Li, X.; Somesfalean, G.; Zhang, Y.; Gao, H.; Zhang, Z. Synthesis and upconversion properties of monoclinic Gd₂O₃: Er³⁺ nanocrystals. *Opt. Mater.* **2008**, *30*, 1284–1288. [[CrossRef](#)]
123. Qin, X.; Yokomori, T.; Ju, Y. Flame synthesis and characterization of rare-earth (Er³⁺, Ho³⁺, and Tm³⁺) doped upconversion nanophosphors. *Appl. Phys. Lett.* **2007**, *90*, 073104. [[CrossRef](#)]
124. Liu, J.; Bu, W.; Pan, L.; Shi, J. NIR-triggered anticancer drug delivery by upconverting nanoparticles with integrated azoben-zene-modified mesoporous silica. *Angew. Chem.* **2013**, *125*, 4471–4475. [[CrossRef](#)]
125. Liu, Y.; Hou, W.; Sun, H.; Cui, C.; Zhang, L.; Jiang, Y.; Wu, Y.; Wang, Y.; Li, J.; Sumerlin, B.S.; et al. Thiol-ene click chemistry: A biocompatible way for orthogonal bioconjugation of colloidal nanoparticles. *Chem. Sci.* **2017**, *8*, 6182–6187. [[CrossRef](#)] [[PubMed](#)]

126. Kong, W.; Sun, T.; Chen, B.; Chen, X.; Ai, F.; Zhu, X.; Li, M.; Zhang, W.; Zhu, G.; Wang, F. A general strategy for ligand exchange on upconversion nanoparticles. *Inorg. Chem.* **2017**, *56*, 872–877. [[CrossRef](#)] [[PubMed](#)]
127. Bao, G.; Wen, S.; Lin, G.; Yuan, J.; Lin, J.; Wong, K.L.; Bünzli, J.C.G.; Jin, D. Learning from lanthanide complexes: The development of dye-lanthanide nanoparticles and their biomedical applications. *Coord. Chem. Rev.* **2020**, *429*, 213642. [[CrossRef](#)]
128. Das, G.K.; Stark, D.T.; Kennedy, I.M. Potential toxicity of up-converting nanoparticles encapsulated with a bilayer formed by ligand attraction. *Langmuir* **2014**, *30*, 8167–8176. [[CrossRef](#)] [[PubMed](#)]
129. Li, X.; Shen, D.; Yang, J.; Yao, C.; Che, R.; Zhang, F.; Zhao, D. Successive layer-by-layer strategy for multi-shell epitaxial growth: Shell thickness and doping position dependence in upconverting optical properties. *Chem. Mater.* **2013**, *25*, 106–112. [[CrossRef](#)]
130. Shen, J.; Li, K.; Cheng, L.; Liu, Z.; Lee, S.T.; Liu, J. Specific detection and simultaneously localized photothermal treatment of cancer cells using layer-by-layer assembled multifunctional nanoparticles. *ACS Appl. Mater. Interfaces* **2014**, *6*, 6443–6452. [[CrossRef](#)]
131. Escudero, A.; Carrillo-Carrión, C.; Zyuzin, M.V.; Parak, W.J. Luminescent rare-earth-based nanoparticles: A summarized overview of their synthesis, functionalization, and applications. *Top. Curr. Chem.* **2016**, *374*, 1–15. [[CrossRef](#)]
132. Lai, W.F.; Rogach, A.L.; Wong, W.T. Molecular design of upconversion nanoparticles for gene delivery. *Chem. Sci.* **2017**, *8*, 7339–7358. [[CrossRef](#)]
133. Xu, C.T.; Zhan, Q.; Liu, H.; Somesfalean, G.; Qian, J.; He, S.; Andersson-Engels, S. Upconverting nanoparticles for pre-clinical diffuse optical imaging, microscopy and sensing: Current trends and future challenges. *Laser Photonics Rev.* **2013**, *7*, 663–697. [[CrossRef](#)]
134. Chen, Z.; Chen, H.; Hu, H.; Yu, M.; Li, F.; Zhang, Q.; Zhou, Z.; Yi, T.; Huang, C. Versatile synthesis strategy for carboxylic acid-functionalized upconverting nanophosphors as biological labels. *J. Am. Chem. Soc.* **2008**, *130*, 3023–3029. [[CrossRef](#)] [[PubMed](#)]
135. Sivakumar, S.; Diamente, P.R.; van Veggel, F.C.J.M. Silica-coated Ln³⁺-doped LaF₃ nanoparticles as robust down-and upconverting biolabels. *Chem. Eur. J.* **2006**, *12*, 5878–5884. [[CrossRef](#)]
136. Yi, G.S.; Chow, G.M. Synthesis of hexagonal-phase NaYF₄: Yb, Er and NaYF₄: Yb, Tm nanocrystals with efficient up-conversion fluorescence. *Adv. Funct. Mater.* **2006**, *16*, 2324–2329. [[CrossRef](#)]
137. Dong, A.; Ye, X.; Chen, J.; Kang, Y.; Gordon, T.; Kikkawa, J.M.; Murray, C.B. A generalized ligand-exchange strategy enabling sequential surface functionalization of colloidal nanocrystals. *J. Am. Chem. Soc.* **2011**, *133*, 998–1006. [[CrossRef](#)] [[PubMed](#)]
138. Zhou, H.P.; Xu, C.H.; Sun, W.; Yan, C.H. Clean and flexible modification strategy for carboxyl/aldehyde-functionalized upconversion nanoparticles and their optical applications. *Adv. Funct. Mater.* **2009**, *19*, 3892–3900. [[CrossRef](#)]
139. Bao, Y.; Luu, Q.A.N.; Lin, C.; Schloss, J.M.; May, P.S.; Jiang, C. Layer-by-layer assembly of freestanding thin films with homogeneously distributed upconversion nanocrystals. *J. Mater. Chem.* **2010**, *20*, 8356–8361. [[CrossRef](#)]
140. Yi, G.S.; Chow, G.M. Water-soluble NaYF₄: Yb, Er (Tm)/NaYF₄/polymer core/shell/shell nanoparticles with significant enhancement of upconversion fluorescence. *Chem. Mater.* **2007**, *19*, 341–343. [[CrossRef](#)]
141. Sharipov, M.; Tawfik, S.M.; Gerelkhuu, Z.; Huy, B.T.; Lee, Y.I. Phospholipase A2-responsive phosphate micelle-loaded UCNPs for bioimaging of prostate cancer cells. *Sci. Rep.* **2017**, *7*, 1–9.
142. Wang, D.; Zhu, L.; Pu, Y.; Wang, J.X.; Chen, J.F.; Dai, L. Transferrin-coated magnetic upconversion nanoparticles for efficient photodynamic therapy with near-infrared irradiation and luminescence bioimaging. *Nanoscale* **2017**, *9*, 11214–11221. [[CrossRef](#)] [[PubMed](#)]
143. Teh, D.B.L.; Bansal, A.; Chai, C.; Toh, T.B.; Tucker, R.A.J.; Gammad, G.G.L.; Yeo, Y.; Lei, Z.; Zheng, X.; Yang, F.; et al. A Flexi-PEGDA Upconversion Implant for Wireless Brain Photodynamic Therapy. *Adv. Mater.* **2020**, *32*, 2001459. [[CrossRef](#)]
144. Wang, C.; Zhao, P.; Yang, G.; Chen, X.; Jiang, Y.; Jiang, X.; Wu, Y.; Liu, Y.; Zhang, W.; Bu, W. Reconstructing the intracellular pH microenvironment for enhancing photodynamic therapy. *Mater. Horiz.* **2020**, *7*, 1180–1185. [[CrossRef](#)]
145. Li, Y.; Zhang, X.; Zhang, Y.; Zhang, Y.; He, Y.; Liu, Y.; Ju, H. Activatable photodynamic therapy with therapeutic effect prediction based on a self-correction upconversion nanoprobe. *ACS Appl. Mater. Interfaces* **2020**, *12*, 19313–19323. [[CrossRef](#)]
146. Zhang, Y.; Chen, W.; Zhang, Y.; Zhang, X.; Liu, Y.; Ju, H. A Near-Infrared Photo-Switched MicroRNA Amplifier for Precise Photodynamic Therapy of Early-Stage Cancers. *Angew. Chem.* **2020**, *132*, 21638–21643. [[CrossRef](#)]
147. Lin, B.; Liu, J.; Wang, Y.; Yang, F.; Huang, L.; Lv, R. Enhanced upconversion luminescence-guided synergistic antitumor therapy based on photodynamic therapy and immune checkpoint blockade. *Chem. Mater.* **2020**, *32*, 4627–4640. [[CrossRef](#)]
148. Li, Z.; Qiao, X.; He, G.; Sun, X.; Feng, D.; Hu, L.; Xu, H.; Xu, H.B.; Ma, S.; Tian, J. Core-satellite metal-organic framework@ upconversion nanoparticle superstructures via electrostatic self-assembly for efficient photodynamic theranostics. *Nano Res.* **2020**, *13*, 3377–3386. [[CrossRef](#)]
149. Sun, X.; Sun, J.; Dong, B.; Huang, G.; Zhang, L.; Zhou, W.; Lv, J.; Zhang, X.; Liu, M.; Xu, L.; et al. Noninvasive temperature monitoring for dual-modal tumor therapy based on lanthanide-doped up-conversion nanocomposites. *Biomaterials* **2019**, *201*, 42–52. [[CrossRef](#)] [[PubMed](#)]
150. Liu, Z.; Xiong, L.; Ouyang, G.; Ma, L.; Sahi, S.; Wang, K.; Lin, L.; Huang, H.; Miao, X.; Chen, W.; et al. The Investigation of Copper Cysteamine Nanoparticles as a new type of radiosensitizers for Colorectal Carcinoma. *Sci. Rep.* **2017**, *7*, 9290. [[CrossRef](#)] [[PubMed](#)]
151. Chen, W.; Zhang, J. Using Nanoparticles to Enable Simultaneous Radiation and Photodynamic Therapies for Cancer Treatment. *J. Nanosci. Nanotechnol.* **2006**, *6*, 1159–1166. [[CrossRef](#)]

152. Chen, W. Nanoparticle Self-Lighting Photodynamic Therapy for Cancer Treatment. *J. Biomed. Nanotechnol.* **2008**, *4*, 369–376. [[CrossRef](#)]
153. Ma, L.; Chen, W.; Schatte, G.; Wang, W.; Joly, A.G.; Huang, Y.; Sammynaiken, R.; Hossu, M. A new Cu–cysteamine complex: Structure and optical properties. *J. Mater. Chem. C* **2014**, *2*, 4239–4246. [[CrossRef](#)]
154. Ma, L.; Zou, X.; Chen, W. A New X-ray Induced Nanoparticle Photosensitizers for Cancer Treatment. *J. Biomed. Nanotechnol.* **2014**, *10*, 1501–1508. [[CrossRef](#)]
155. Shrestha, S.; Wu, J.; Sah, B.; Vanasse, A.; Cooper, L.N.; Ma, L.; Li, G.; Zheng, H.; Chen, W.; Antosh, M.P. X-ray induced photodynamic therapy with copper-cysteamine nanoparticles in mice tumors. *Proc. Natl. Acad. Sci. USA* **2019**, *116*, 16823–16828. [[CrossRef](#)] [[PubMed](#)]
156. Shi, L.; Liu, P.; Wu, J.; Ma, L.; Zheng, H.; Antosh, M.P.; Zhang, H.; Wang, B.; Chen, W.; Wang, X. The effectiveness and safety of copper-cysteamine nanoparticle mediated X-PDT for cutaneous squamous cell carcinoma and melanom. *Nanomedicine* **2019**, *14*, 2027–2043. [[CrossRef](#)]
157. Zhang, Q.; Guo, X.; Cheng, Y.; Chudal, L.; Pandey, N.K.; Zhang, J.; Ma, L.; Xi, Q.; Yang, G.; Chen, Y.; et al. Use of copper-cysteamine nanoparticles to simultaneously enable radiotherapy oxidative therapy and immunotherapy for melanoma treatment. *Signal Transduct. Target. Ther.* **2020**, *5*, 58. [[CrossRef](#)]
158. Sah, B.; Wu, J.; Vanasse, A.; Pandey, N.K.; Chudal, L.; Huang, Z.; Song, W.; Yu, H.; Ma, L.; Chen, W.; et al. Effects of Nanoparticle Size and Radiation Energy on Copper-Cysteamine Nanoparticles for X-ray Induced Photodynamic Therapy. *Nanomaterials* **2020**, *10*, 1087. [[CrossRef](#)]
159. Chen, X.; Liu, J.; Li, Y.; Pandey, N.K.; Chen, T.; Wang, L.; Amador, E.H.; Chen, W.; Liu, F.; Xiao, E.; et al. Study of copper-cysteamine based X-ray induced photodynamic therapy and its effects on cancer cell proliferation and migration in a clinical mimic setting. *Bioact. Mater.* **2021**, *7*, 504–514. [[CrossRef](#)]
160. Wang, Y.; Alkhalidi, N.D.; Pandey, N.K.; Chudal, L.; Wang, L.Y.; Lin, L.W.; Zhang, M.B.; Yong, Y.X.; Amador, E.H.; Huda, M.N.; et al. A new type of cuprous-cysteamine sensitizers: Synthesis, optical properties and potential applications. *Mater. Today Phys.* **2021**, *19*, 100435. [[CrossRef](#)]
161. Liu, F.; Chen, W.; Wang, S.P.; Joly, A.G. Investigation of Water-Soluble X-ray Luminescence Nanoparticles For Photodynamic Activation. *Appl. Phys. Lett.* **2008**, *92*, 43901. [[CrossRef](#)]
162. Liu, Z.; Xiong, L.; Ouyang, G.; Ma, L.; Sahi, S.; Wang, K.; Lin, L.; Huang, H.; Miao, X.; Chen, W.; et al. Investigation of copper-cysteamine nanoparticles as a new photosensitizer for an-ti-hepatocellular carcinoma. *Cancer Biol. Ther.* **2019**, *20*, 812–825.
163. Pandey, N.K.; Chudal, L.; Phan, J.; Lin, L.; Johnson, O.; Xing, M.; Liu, J.P.; Li, H.; Huang, X.; Shu, Y.; et al. A facile method for synthesis of copper-cysteamine nanoparticles and study of ROS production for cancer treatment. *J. Mater. Chem. B* **2019**, *7*, 6630–6642. [[CrossRef](#)] [[PubMed](#)]